JACS
JOURNAL OF THE AMERICAN CHEMICAL SOCIETY
Article
pubs.acs.org/JACS

Direct Visualization of Excited-State Symmetry Breaking Using Ultrafast Time-Resolved Infrared Spectroscopy

Bogdan Dereka,[†] Arnulf Rosspeintner,[†] Zhiquan Li,[‡,§] Robert Liska,[‡] and Eric Vauthey*[,†]

[†]Department of Physical Chemistry, University of Geneva, 30 Quai Ernest-Ansermet, CH-1211 Geneva 4, Switzerland
[‡]Institute of Applied Synthetic Chemistry, Vienna University of Technology, Getreidemarkt 9/163/MC, 1060 Vienna, Austria

Supporting Information

ABSTRACT: Most symmetric quadrupolar molecules designed for two-photon absorption behave as dipolar molecules in the S_1 electronic excited state. This is usually explained by a breakup of the symmetry in the excited state. However, the origin of this process and its dynamics are still not fully understood. Here, excited-state symmetry breaking in a quadrupolar molecule with a D-π-A-π-D motif, where D and A are electron donating and accepting units, is observed in real time using ultrafast transient infrared absorption spectroscopy. The nature of the relaxed S_1 state was found to strongly depend on the solvent polarity: (1) in nonpolar solvents, it is symmetric and quadrupolar; (2) in weakly polar media, the quadrupolar state observed directly after excitation transforms to a symmetry broken S_1 state with one arm bearing more excitation than the other; and (3) in highly polar solvents, the excited state evolves further to a purely dipolar S_1 state with the excitation localized entirely on one arm. The time scales associated with the transitions between these states coincide with those of solvation dynamics, indicating that symmetry breaking is governed by solvent fluctuations.

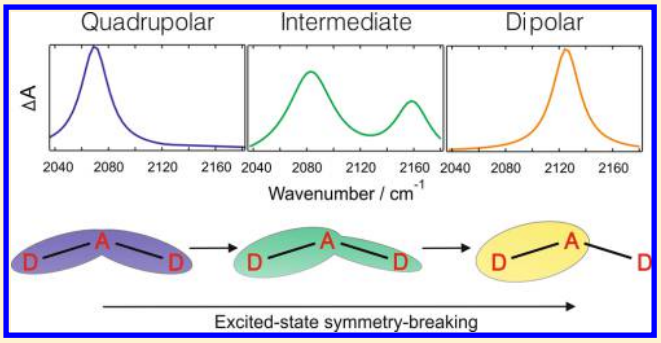

INTRODUCTION

Molecules with a large two-photon absorption cross-section, δ, are highly demanded for numerous applications ranging from photopolymerization to bioimaging and photodynamic therapy.[1−14] As large δ is associated with significant changes of electric quadrupolar or octupolar moments upon excitation,[15−19] most of the high δ molecules synthesized so far contain several electron donor/acceptor (D/A) units arranged in D(-π-A)$_n$ or A(-π-D)$_n$ (n = 2, 3) motifs. A generally good understanding of the properties of these multibranched DA systems in the electronic ground state has been achieved thanks to numerous investigations on the relationship between δ and their multipolar character, their symmetry, and their one-photon absorption spectra.[20−26] However, the same cannot be said for their excited states: whereas the electronic absorption spectra of multibranched DA molecules do not present a significant solvent dependence, as expected for a purely quadrupolar or octupolar ground state, the fluorescence spectra exhibit a strong solvatochromism indicative of a dipolar S_1 state.[21−23,27−29] This striking phenomenon has been explained in terms of a breakup of the symmetry in the excited state driven by structural and/or solvent fluctuations.[30−34]

Although this idea is generally accepted, a real-time observation of this excited-state symmetry breaking is still missing. This would not only give a firm ground to this hypothesis but also unveil the origin of the process, namely structural and/or solvent fluctuations. Time-resolved electronic spectroscopy does not give direct insight into the origin of the symmetry breaking as, in the experiments reported so far, the excited-state dynamics of multibranched molecules was found to be alike that of their single branch analogues.[28,29,35,36]

Here, we report on the real-time visualization of the symmetry-breaking dynamics upon photoexcitation of a quadrupolar D-π-A-π-D molecule (**DAD**, Chart 1) using femtosecond time-resolved infrared (TRIR) spectroscopy. This molecule, developed as a photoinitiator for two-photon

Chart 1. Structure of DAD and DA[a]

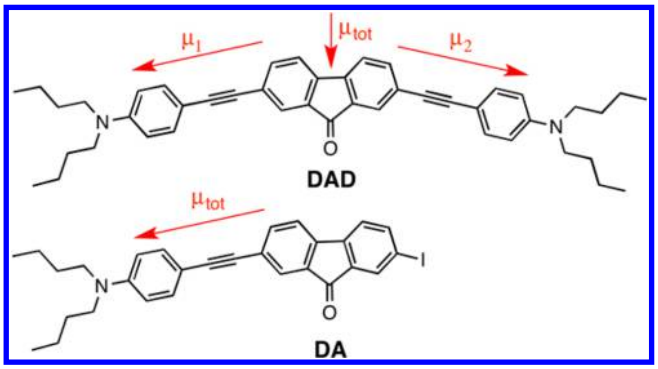

[a]The red arrows are qualitative representations of the local and total permanent electric dipole moments.

Received: February 5, 2016
Published: March 17, 2016

DOI: 10.1021/jacs.6b01362
J. Am. Chem. Soc. 2016, 138, 4643−4649

induced polymerization,[37] is close to linear and comprises a central fluorenone acceptor flanked by two branches consisting of an aromatic dibutylamine donor linked via an acetylene bridge. It contains several IR marker modes, such as −C≡C−, −C═C−, and −C═O stretches, that can be probed to monitor the temporal evolution of the excited state in different regions of the molecule. The −C≡C− stretch is particularly convenient as it is a highly localized vibration, present in both arms and with a frequency well separated from those of the other modes. Access to the symmetry breaking dynamics has been obtained by monitoring the IR spectrum in the −C≡C− stretch region at different times after photoexcitation. When the electronic structure of **DAD** is symmetric, the electronic distribution is the same in both arms and a single −C≡C− band is observed. However, an uneven distribution of the excitation results in two different −C≡C− stretch frequencies.

RESULTS AND DISCUSSION

Steady-State and Time-Resolved Electronic Spectroscopy. A first check of the occurrence of symmetry breaking in the excited state was carried out by measuring the solvent dependence of the electronic absorption and emission spectra of **DAD** and of its single branch D-π-A analogue (**DA**, Chart 1). The former exhibits almost no solvatochromism in absorption (Figure 1A) but a strong one in emission, the fluorescence maximum shifting by 2350 cm^{-1} upon going from cyclohexane (CHX, dielectric constant ε_s = 2, Table S1, Supporting Information) to propylacetate (PA, ε_s = 6).

In fact, the fluorescence spectrum shifts to the near-IR (λ_{max} > 840 nm) already in moderately polar solvents. Additionally, the fluorescence quantum yield decreases substantially when increasing the solvent polarity, varying from 0.4 in CHX to 0.01 in PA (Table S2). Therefore, the solvatochromism of the fluorescence could only be investigated in a limited range of solvent polarity. A weak solvent dependence of the absorption spectrum can also be observed with the single branch analogue **DA** (Figure S1). Fluorescence exhibits even a larger solvatochromism than that for **DAD**, with the band maximum shifting by 2520 cm^{-1} upon going from CHX to PA.

These results reveal that, in polar solvents at least, the electronic structure of **DAD** in the S_1 state should not differ much from that of **DA**, and should thus have a strong dipolar character. As the angle between the two arms of **DAD** is around 160°, a delocalized and symmetric S_1 state would be weakly polar, because the dipole moments localized on both arms would be the same and almost cancel ($\mu_1 = \mu_2$, Chart 1).

The one- and two-photon absorption spectra of **DAD** are compared in Figure 1B and are discussed in detail in the Supporting Information (Figures S2−S5). They reveal that the $S_1 \leftarrow S_0$ transition ($\lambda_{max} \sim 475$ nm) is one-photon allowed and two-photon forbidden, whereas the $S_2 \leftarrow S_0$ transition ($\lambda_{max} \sim 410$ nm) is one-photon forbidden and two-photon allowed. Such a behavior is characteristic of a quasi-centrosymmetric quadrupolar molecule.[23,38]

All these results indicate that both the ground state and the FC excited states of **DAD** are symmetric ($\mu_1 = \mu_2$) and quadrupolar and that symmetry breaking to the dipolar S_1 state ($\mu_1 \neq \mu_2$) occurs after population of the FC state.

No insight into the dynamics of the symmetry breaking could be obtained from transient electronic absorption measurements of **DAD** and **DA**. Figure 2 shows that the shape of the transient spectra measured upon 400 nm excitation of **DAD** is essentially the same that in CHX and dimethyl sulfoxide (DMSO).

Detailed analysis of these spectra and those in solvents of intermediate polarity is presented in the Supporting Informa-

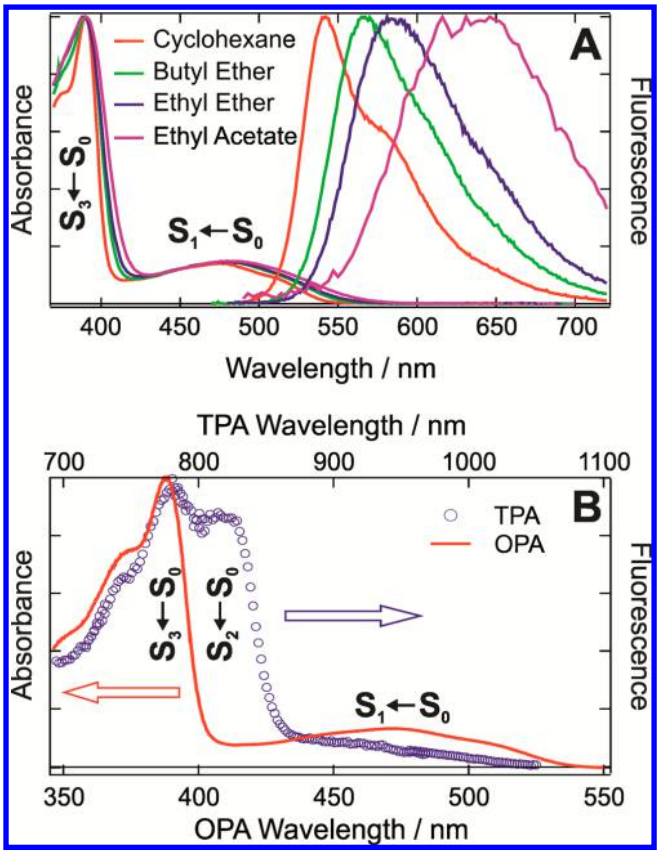

Figure 1. (A) Solvent dependence of the electronic absorption and fluorescence spectra of **DAD** and (B) linear electronic absorption spectrum (OPA, ε(400 nm) = 10^5 M^{-1} cm^{-1})[37] and two-photon fluorescence excitation spectrum (TPA, δ(800 nm) = 440 GM)[37] of **DAD** in *n*-hexane.

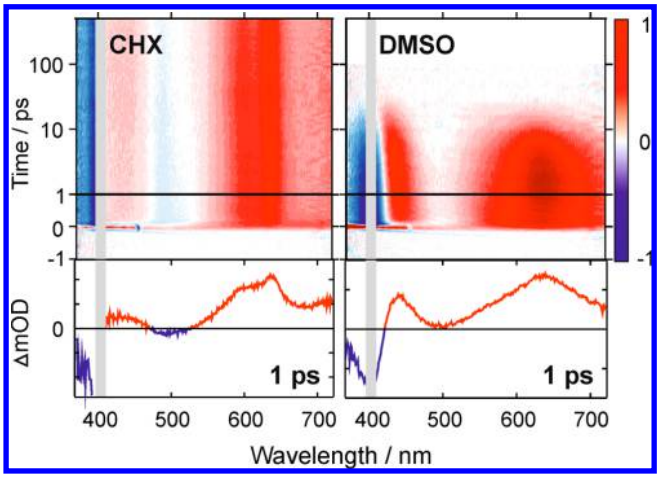

Figure 2. Temporal evolution of the transient electronic absorption recorded upon 400 nm excitation of **DAD** in cyclohexane (CHX) and dimethyl sulfoxide (DMSO) and transient spectra recorded 1 ps after excitation (bottom). The positive bands (red) are due to excited-state absorption (ESA), whereas the negative bands originate from the bleach of the $S_1 \leftarrow S_0$ and $S_3 \leftarrow S_0$ absorption.

DOI: 10.1021/jacs.6b01362
J. Am. Chem. Soc. 2016, 138, 4643−4649

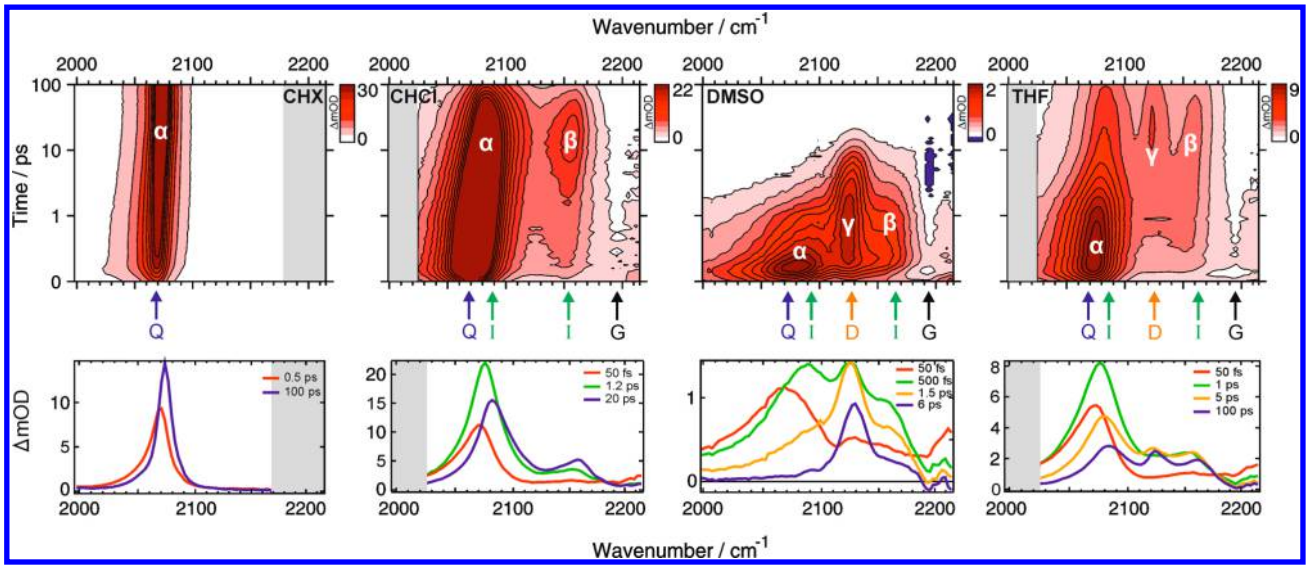

Figure 3. Temporal evolution of the transient infrared absorption recorded upon 400 nm excitation of **DAD** in solvents of increasing polarity (top) and transient spectra measured at selected time delays (bottom). The bands are designated using Greek letters (α to γ) and assigned to different states/transients (*Q*, quadrupolar state; *I*, intermediate state; *D*, dipolar state; *G*, ground state, see text).

tion (Figures S6 and S7). The lifetime of the S_1 state of **DAD** displays a large solvent dependence and decreases from 4.9 ns in CHX to 7.2 ps in DMSO (Table S3). This behavior is consistent with the energy gap law of nonradiative transitions,[39,40] as shown by the good correlation between the lifetime and the S_1-S_0 gap (Figure S8). Considering the charge-transfer character of the S_1 state, this solvent dependence can also be qualitatively accounted for in terms of Marcus theory.[41] Lowering the solvent polarity increases the driving force and decreases solvent reorganization energy. Consequently, charge recombination slows down because it occurs deeper in the inverted region.

The transient electronic absorption spectra recorded with the single branch analogue, **DA**, are qualitatively similar to those measured with **DAD** (Figure S9). Additionally, the excited-state lifetime of **DA** also shortens with increasing solvent polarity.

Despite useful information on the excited-state lifetime, these transient electronic absorption data do not present any clear feature that could be assigned to the transition from a symmetric and quadrupolar excited state to an asymmetric dipolar state. They seem to rather confirm the dipolar nature of the S_1 state already deduced from the solvatochromism.

TRIR Absorption Spectra. Direct insight into the nature of the excited state was obtained by probing the electronic density at the center of each A-π-D arm using TRIR spectroscopy. Figure 3 shows the time evolution of the transient absorption measured in the $-C\equiv C-$ stretch region after 400 nm excitation of **DAD** in solvents of varying polarity. TRIR data measured in other solvents (dibutyl ether, diethyl ether, benzonitrile and acetonitrile) are shown in Figure S12.

In general, the TRIR spectra are dominated by excited-state absorption (ESA) bands and only weak ground-state bleach around 2195 cm^{-1} can be discerned. Contrary to the transient electronic absorption spectra, these transient IR spectra exhibit a remarkable solvent dependence. In the nonpolar CHX, the spectrum exhibits a single, very intense band around 2070 cm^{-1} denoted from now on band α. During the first 10−15 ps after excitation, this band raises, upshifts by 5 cm^{-1} and narrows on the low-frequency side, before decaying partially within the 2 ns experimental window. In $CHCl_3$, the earliest transient spectra contain band α together with a hardly visible band around 2150−2160 cm^{-1} that will be called band β. Band α undergoes similar early dynamics as in CHX, but with a larger frequency upshift (~11 cm^{-1}). Meanwhile, band β rises and shifts to higher frequency within 20 ps. Afterward, both bands decay simultaneously to zero within 400 ps. Similar spectral dynamics can be observed in the other weakly polar dibutyl and diethyl ether (Figure S12). In the most polar DMSO, a third band located at 2130 cm^{-1}, band γ, is present at early time as well. While bands α and β decay entirely to zero, the first faster than the second, band γ increases further during the first few picoseconds before decaying to zero on a slower time scale. After ~15 ps, band γ is the only ESA band visible in this spectral region. A qualitatively similar behavior is observed in other highly polar solvents, benzonitrile and acetonitrile (Figure S12). In the latter, however, spectral evolution is much faster and band γ is the only transient feature visible after 1 ps.

The most complicated spectra are observed in the medium polar THF: first, band α undergoes a partial decay while both bands β and γ rise, the former faster than the latter; afterward, all three bands decay simultaneously within ~1 ns.

Assignment of the ESA Bands. The spectra in CHX with a single and intense band are consistent with a symmetric quadrupolar excited state, called from now on state *Q*. Band α can be assigned to the asymmetric $-C\equiv C-$ stretch vibration of **DAD** in the S_1 state. The huge absorption coefficient of this band (about 3×10^5 M^{-1} cm^{-1}) can be explained by the considerable change of dipole moment associated with this asymmetric concerted vibrational motion of both ethyne bonds and by a possible coupling with the close-by one-photon allowed electronic $S_2 \leftarrow S_1$ transition.[42,43] The increase, shift, and narrowing of the band observed at early time can be attributed to vibrational relaxation processes.[44−46] Excitation at 400 nm results in the population of an upper excited state $S_{n>1}$, most probably the S_3 state, and is followed by an ultrafast internal conversion to the S_1 state. During this process, about 0.7 eV excess energy is redistributed into vibrational modes of the molecule before being dissipated into the environment. The time constants associated with this early dynamics obtained from global target analysis coincide with those obtained from

DOI: 10.1021/jacs.6b01362
J. Am. Chem. Soc. 2016, 138, 4643−4649

the transient electronic absorption data (Tables S3 and S5). Similarly, the slow decay of band α agrees with the nanosecond lifetime of the S_1 state in CHX.

In $CHCl_3$, the frequency upshift of band α is more than twice as large as that in CHX and the high-frequency side of this band broadens distinctly during the rise of band β. This strongly suggests that, in this solvent, two different states/species contribute to band α: the same quadrupolar state Q that is also observed in CHX and another state that is also responsible for band β. For reasons that will appear clearer below, this second state will be called intermediate state, state I. In consequence, the dynamics observed in $CHCl_3$ can be explained by a transition from state Q to state I, followed by the decay from state I. This scenario is also supported by the evolution-associated difference absorption spectra (EADS)[47] resulting from a global target analysis assuming a series of consecutive exponential steps (Table S5 and Figure S13). The lifetime of the state I, 100 ps, coincides with the S_1 state lifetime obtained from the transient electronic absorption measurements. The presence of two distinct −C≡C− stretch bands in the spectrum of state I is an unambiguous indication that the electronic densities in both branches differ ($\mu_1 \neq \mu_2$) and that this state is no longer symmetric. Here, state I is the equilibrated S_1 state, whereas state Q corresponds to the lowest symmetric excited state populated upon internal conversion from the FC $S_{n>1}$ state.

The $Q \rightarrow I$ transition is also occurring in the most polar solvents, DMSO and benzonitrile. It appears as a 10 cm^{-1} frequency upshift of band α and a concomitant rise of band β. Here, however, this process is followed by a transition to a third state with a single −C≡C− stretch band around 2130 cm^{-1} (band γ) and a lifetime coinciding with that of the S_1 state.

These data reveal that the nature of the S_1 state of **DAD** changes drastically upon increasing solvent polarity. It is symmetric and highly quadrupolar in nonpolar solvents and becomes asymmetric when going to the weakly polar $CHCl_3$ and ethers with a higher density of the excitation, i.e., a larger charge-transfer character, on one branch.

The TRIR spectra measured with the dipolar **DA** allow unambiguous assignment of band γ observed in the most polar solvents (Figures 4 and S18). These spectra consist of a negative band at about 2190 cm^{-1} due to the ground-state bleach and of a single ESA band centered around 2130 cm^{-1}, independently of the solvent polarity (Figures 4 and S18). This band exhibits some initial shift and narrowing, which can be assigned to vibrational relaxation similarly to **DAD**, and then decays with the same time constant as that obtained from the transient electronic absorption measurements. This single ESA band due to the −C≡C− stretch of **DA** in the S_1 state is at the same frequency as band γ of **DAD** (Figure 3). Therefore, band γ can be assigned to a purely dipolar excited state, state D, with the excitation entirely localized on a single arm of **DAD**. This is a fully symmetry broken state, and consequently, whereas the −C≡C− stretch frequency of the excited branch is the same as that measured with **DA**, the frequency of the other branch should coincide with that of **DAD** or **DA** in the ground state and should be located around 2190 cm^{-1}. This band is not visible in the transient spectra because it coincides with the ground-state bleach. In principle, the $I \rightarrow D$ transition should lead to a partial recovery of the ground-state bleach. Unfortunately, the bleach is hardly visible because it is extremely weak and overlaps with ESA bands, especially band β.

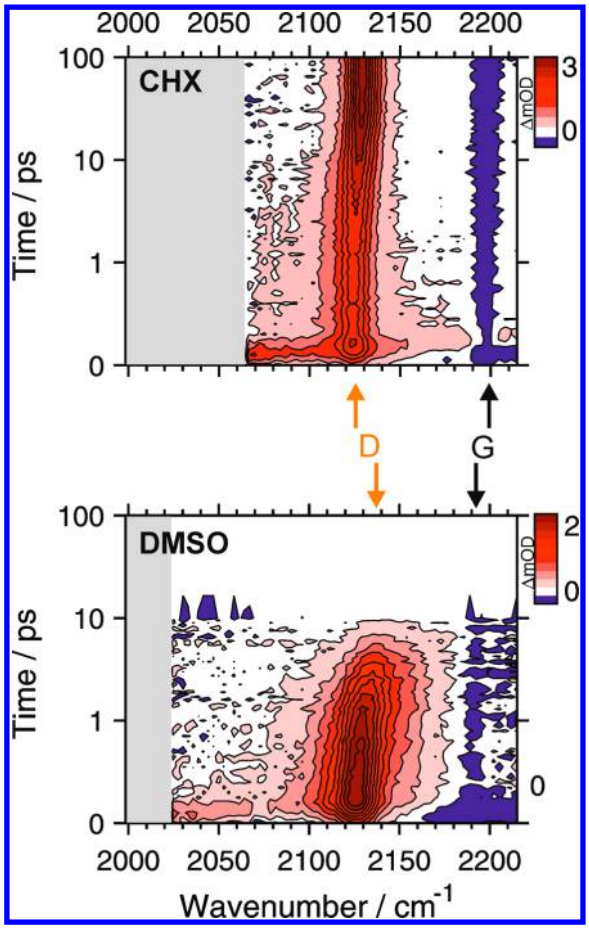

Figure 4. Temporal evolution of the transient infrared absorption recorded upon 400 nm excitation of **DA** in cyclohexane (CHX) and dimethyl sulfoxide (DMSO) and band assignment (*D*, dipolar state; *G*, ground state).

The TRIR spectra measured in medium polar THF (Figure 3) can now be rationalized. After excitation and ultrafast internal conversion, the $Q \rightarrow I$ transition takes place, as testified by the shift of band α and the rise of band β. The slower buildup of band γ (state D) followed by the parallel decay of all three bands points to the establishment of an equilibrium between states I and D.

Frequency Downshift of the ESA Bands. Regardless of the nature of the excited state, all three bands, namely α, β, and γ, are frequency downshifted relative to the ground-state bleach. This downshift, $-\Delta\tilde{\nu}$, is consistent with the π–π^* character of the excited state and reflects the decrease of the ethyne bond order. As shown in Table 1, $-\Delta\tilde{\nu}$ decreases significantly when going from state Q to state I and state D, indicating that the

Table 1. −C≡C− Stretch Frequencies of DAD in Different States and Frequency Downshift, $-\Delta\tilde{\nu}$, Relatively to the Ground State[a]

state	$\tilde{\nu}$(C≡C)/ cm^{-1}	$-\Delta\tilde{\nu}$/ cm^{-1}
G	2190	0
Q	2073	117
I	2082, 2158	108, 32
D	2130	60

[a] *G*, ground state; *Q*, quadrupolar state; *I*, intermediate state; *D*, dipolar state.

DOI: 10.1021/jacs.6b01362
J. Am. Chem. Soc. 2016, 138, 4643−4649

ethyne bond order increases with increasing charge-transfer character of the excited state. This is consistent with the observation by Weinstein and co-workers that the frequency downshift of the −C≡C− stretch of a series of Pt-based D-π-A compounds upon optical excitation decreases with increasing electron donating strength of the push group.[48] To further confirm the correlation between the amount of charge transfer in an A-π-D branch and the frequency downshift, quantum-chemical calculations have been performed with a series of phenylethynylbenzene push−pull derivatives with a cyano accepting group on one end and various electron-donating groups at the other end (Figure S23). With all donors, the −C≡C− frequency is smaller in the excited than in the ground state, as expected for a $\pi-\pi^*$ excitation. However, this frequency downshift diminishes and the ethyne bond shortens with increasing dipolar character of the excited state. This can be rationalized by considering that, upon increasing the strength of the push−pull groups, the HOMO and LUMO become progressively more localized on the donor and acceptor units, respectively, and consequently, the bond order of the ethyne bridge becomes gradually less affected by excitation. Therefore, the smaller downshift observed with state *D* is consistent with the larger dipolar character of this state due to the localization of the excitation on a single branch.

The assignment of the two bands of state *I* deserves some attention. This state is interpreted as an asymmetric state with more excitation on one arm. Consequently, the dipolar character of this state should be between those of state *Q* and state *D*. The 2082 cm^{-1} band is consistent with this interpretation and can be attributed to the vibration in the branch bearing most of the excitation. As a consequence, because of the low density of excitation on the ethyne bond in the other branch and, thus, of the small decrease of bond order relatively to the ground state, the frequency downshift of the second −C≡C− band of state *I* should be small, in full agreement with the band observed at 2158 cm^{-1} ($-\Delta\tilde{\nu}$ = 32 cm^{-1}). Furthermore, the intensity of this second band is much weaker than that of the 2082 cm^{-1} band, because the local dipole moment of this arm is smaller than that of the arm bearing most of the excitation.

To summarize, the transient vibrational absorption data reveal that 400 nm excitation is followed by ultrafast internal conversion to the lowest symmetric excited state, state *Q*. In nonpolar media, this state is the lowest singlet excited state of **DAD** and decays on the nanosecond time scale. In weakly polar solvents, state *Q* evolves into an asymmetric state, state *I*, where excitation is no longer evenly distributed on both branches, and in the most polar solvents, state *I* converts in turn into a totally asymmetric and dipolar state, state *D*. The nature of the S_1 state of **DAD** is, thus, entirely determined by the polarity of the environment.

Spectral Dynamics. The time scales associated with these transitions were determined using two approaches, which yielded qualitatively similar results: (i) global target analysis assuming consecutive exponential steps (Figure S13) and (ii) band-shape analysis of the transient spectra using a sum of Lorentzian functions followed by a multiexponential analysis of the time evolution of the band areas (Figures S14−S17). The parallel changes of band shape and intensity indicate that vibrational/solvent relaxation and population dynamics are closely entangled and that the time constants obtained from any of these approaches cannot be associated with a single process but should rather be considered as representative time scales of the overall dynamics. The same is true for the spectra obtained from global analysis (Figure S13) that are evolution-associated rather than species-associated difference absorption spectra.[47]

With this in mind, we can see that the $Q \rightarrow I$ transition in $CHCl_3$ occurs on a similar time scale as that of solvent relaxation (Tables 2 and S1).[49] In DMSO, the $Q \rightarrow I$ and $I \rightarrow D$ transitions mostly take place on an 800 fs and 2.5 ps time scale, respectively (Table 2). These time constants coincide well with those reported for solvation in DMSO (Table S1), with the shorter corresponding to inertial solvent motion and the larger to diffusive motion, each process contributing to about 50% of the total solvation energy.[49] A similar correlation can be found with the other polar solvents, benzonitrile and acetonitrile. In the latter case, solvation is so fast (≤600 fs) that states *Q* and *I* can hardly be discerned.

Table 2. Time Constants Obtained from a Global Analysis of the TRIR Data Measured with DAD and Assignment to the Most Significant Process[a]

solvent	τ_1/ps	τ_2/ps	τ_3/ps
Cyclohexane	0.8, VR	11, VR	4900, $Q \rightarrow G$
Chloroform	0.9, VR	7.9, $Q \rightarrow I$	100, $I \rightarrow G$
Tetrahydrofuran	0.45, $Q \rightarrow I$	2.8, $I \rightarrow D$	350, $I, D \rightarrow G$
Benzonitrile	1.7, $Q \rightarrow I$	6.4, $I \rightarrow D$	41, $D \rightarrow G$
Acetonitrile	0.3, QI → D	3.8, $D \rightarrow G$	
Dimethyl sulfoxide	0.8, $Q \rightarrow I$	2.5, $I \rightarrow D$	6.6, $D \rightarrow G$

[a]VR, vibrational relaxation, *Q*, quadrupolar state, *I*, intermediate state, *D*, dipolar state, *G*, ground state.

TRIR measurements were also performed in the 1450−1650 and 1650−1800 cm^{-1} regions to monitor the aromatic −C═C− and the −C═O stretching modes (Figures S21 and S22). As discussed in the Supporting Information, these spectra do not give much insight into the symmetry breaking process. This is not surprising because the −C═C− stretching modes are delocalized over the entire molecule and the −C═O stretching mode is localized on the central fluorenone and is not sensitive to the electronic distribution in the arms.

Symmetry Breaking Mechanism. We can thus conclude that the observed excited-state symmetry breaking of **DAD** is governed by solvation. This process can be described as follows: although in state *Q* **DAD** is symmetric, the instantaneous orientation of the solvent molecules around both arms at a given time is not the same. This has little consequence in nonpolar solvents, where the solvent field perceived by each branch is equally weak. In this case, excitation remains delocalized over the whole molecule during the lifetime of the S_1 state. The situation is different in polar environments, where the local field around both arms just after excitation may differ significantly. Because of this, the local dipole moment of one branch is better solvated than the other, and consequently, an asymmetric distribution of the excitation is energetically favored. As long as this difference of solvation energy between the two arms does not exceed thermal energy, solvent fluctuations can reverse this process. However, this small initial asymmetry increases further as the solvent reorients along the field generated by the more polar branch. This, in turn, leads to a larger difference in the local field and further localization of the excitation on this branch, i.e., a larger difference between the two local dipole moments μ_1 and μ_2. Our results reveal that, in highly polar solvents, the reaction

DOI: 10.1021/jacs.6b01362
J. Am. Chem. Soc. 2016, 138, 4643−4649

field is strong enough to fully localize the excitation on one arm. This process occurs stepwise: state *I*, where excitation is asymmetrically distributed on both branches is first populated via a partial relaxation of the solvent occurring by inertial motion; further solvent relaxation via diffusive motion leads to a full localization of the excitation on one branch and to the population of state *D*.

In weakly polar media ($CHCl_3$ and ethers), the solvent field is not strong enough, even after complete relaxation, to fully trap the excitation on one arm, and thus, only state *I* is observed. Finally, THF on the one hand is polar enough to allow localization on a single branch, but on the other hand, not sufficiently polar to make it irreversible, and thus, equilibrium between states *I* and *D* is observed.

Although they are not at the origin of symmetry breaking in **DAD**, intramolecular modes play a significant role. Indeed, the states *Q*, *I*, and *D* identified here are not only characterized by different electronic distributions, but have distinct geometries. In an adiabatic picture, these states should correspond to local energy minima on the lowest singlet excited-state potential, and the $Q \rightarrow I$ and $I \rightarrow D$ transitions should be viewed as partial charge-transfer processes. If this were not the case, the $Q \rightarrow I$ and $I \rightarrow D$ transitions would in fact correspond to relaxation processes from a nonequilibrium state and should thus appear as continuous band shifts, similar to the well-known dynamic Stokes shift of the fluorescence upon solvent relaxation, rather than as a decay and rise of bands located at well-defined frequencies. Therefore, the solvent causes an asymmetry in the electronic distribution, which itself triggers an asymmetry in the geometry of **DAD** via structural relaxation.

This is summarized in Figure 5 that illustrates the influence of the solvent on the nature of the S_1 state of **DAD**. In nonpolar

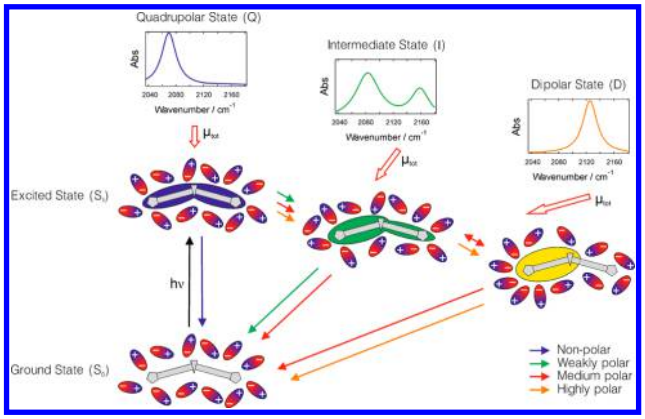

Figure 5. Schematic representation of the effect of the solvent on the nature of the lowest singlet excited state of **DAD**. The colored arrows indicate the pathways of the excited state according to the solvent polarity. The empty arrows represent the total electric dipole moment. The simulated infrared absorption spectra of the different excited states are based on the band shape analysis of the transient spectra in the −C≡C− stretch region.

solvents, this state is highly quadrupolar with a symmetric electronic distribution, i.e., with the same partial charge on both donor ends ($\mu_1 = \mu_2$). In polar solvents, the quadrupolar field of **DAD** in state *Q* polarizes the surrounding solvent, which in turn generates a reaction field. Because of the solvent fluctuations, this field at a given instant is never totally symmetric and one side of **DAD** experiences a stronger field than the other. This asymmetric field favors an asymmetric electronic distribution, i.e., a larger charge-transfer character in the better solvated arm, which can, in turn, polarize the solvent further. This process is accompanied by structural relaxation and leads to state *I*, which is characterized by an asymmetric distribution of the excitation and a distinctly different structure than state *Q*. In the most polar solvents, the reaction field is stronger and more asymmetric, and thus, state *I* evolves to the purely dipolar state *D* where charge transfer only takes place in one arm. As a consequence, whereas state *Q* is the lowest excited state in apolar solvents, states *I* and *D* are progressively stabilized as solvent polarity increases (Figure S24). In THF, states *I* and *D* have similar energies and equilibrium is observed. As solvent polarity increases further, state *D* becomes the lowest excited state.

CONCLUSIONS AND OUTLOOK

We were able to track the charge flow in a symmetric D-π-A-π-D molecule upon photoexcitation and to determine the mechanism and the dynamics of the excited-state symmetry breaking. For this, we used TRIR spectroscopy to monitor vibrational modes of the π-bridge in each D-π-A arm. Contrary to electronic spectroscopy, which probes the entire molecule including the surrounding solvent and, thus, is not able to clearly resolve the spatial distribution of the excitation, vibrational spectroscopy allows probing the electronic distribution with submolecular spatial resolution, provided localized vibrational modes, such as the −C≡C− stretch vibrations, are monitored.

We found that the solvent, via its dielectric properties, plays a pivotal role in both the extent of the symmetry breaking and its dynamics. Therefore, the nature of the emissive state can be tuned by choosing a solvent with an adequate dielectric constant and relaxation dynamics.

This process should be universal for any symmetric molecular architecture with a high order multipolar electronic distribution, i.e., from relatively small molecules with a simple D-π-A-π-D motif, as that investigated here, to larger systems such as dendrimers and conjugated polymers. This symmetry breaking leads to a concentration of the excitation energy. This effect may open new avenues for light harvesting applications with large multipolar conjugated systems.

The understanding achieved here is also relevant for symmetric conjugated systems in rigid environments. In this case, controlling the degree of asymmetry of the surrounding, for example a protein, a supramolecular cage, or an interface, can be used to fine-tune the optical properties, both linear and nonlinear, as well as the excited-state dynamics of conjugated systems and, thus, their photochemistry. A further level of control using selective vibrational excitation, as recently reported for electron transfer reactions,[50] could also be envisioned.

ASSOCIATED CONTENT

Supporting Information

The Supporting Information is available free of charge on the ACS Publications website at DOI: 10.1021/jacs.6b01362.

Experimental details, electronic spectra of **DA**, additional transient electronic and vibrational spectra of **DAD** and **DA** and result of global and band shape analysis, quantum chemistry calculations, estimation of the extinction coefficient of the − C≡C− band (PDF)

DOI: 10.1021/jacs.6b01362
J. Am. Chem. Soc. 2016, 138, 4643−4649

AUTHOR INFORMATION

Corresponding Author

*eric.vauthey@unige.ch

Present Address

§The Key Laboratory of Food Colloids and Biotechnology, School of Chemical and Material Engineering, Jiangnan University, Wuxi, Jiangsu 214122, P. R. China.

Notes

The authors declare no competing financial interest.

ACKNOWLEDGMENTS

This work was supported by the Fonds National Suisse de la Recherche Scientifique through project No. 200020-147098, the University of Geneva and the National Nature Science Foundation of China (21404048).

REFERENCES

(1) Albota, M.; Beljonne, D.; Bredas, J. L.; Ehrlich, J. E.; Fu, J.-Y.; Heikal, A. A.; Hess, S. E.; Kogej, T.; Levin, M. D.; Marder, S. R.; McCord-Maughon, D.; Perry, J. M.; Röckel, H.; Rumi, M.; Subramanian, G.; Webb, W. W.; Wu, X.-L.; Wu, C. *Science* **1998**, *281*, 1653−1656.

(2) Kawata, S.; Sun, H.-B.; Tanaka, T.; Takada, K. *Nature* **2001**, *412*, 697−698.

(3) Lee, K.-S.; Yang, D.-Y.; Park, S. H.; Kim, R. H. *Polym. Adv. Technol.* **2006**, *17*, 72−82.

(4) LaFratta, C. N.; Fourkas, J. T.; Baldacchini, T.; Farrer, R. A. *Angew. Chem., Int. Ed.* **2007**, *46*, 6238−6258.

(5) Walker, E.; Rentzepis, P. M. *Nat. Photonics* **2008**, *2*, 406−408.

(6) Obata, K.; El-Tamer, A.; Koch, L.; Hinze, U.; Chichkov, B. N. *Light: Sci. Appl.* **2013**, *2*, e116.

(7) Cumpston, B. H.; Ananthavel, S. P.; Barlow, S.; Dyer, D. L.; Ehrlich, J. E.; Erskine, L. L.; Heikal, A. a.; Kuebler, S. M.; Lee, I.-Y. S.; McCord-Maughon, D.; Qin, J.; Röckel, H.; Rumi, M.; Wu, X.-L.; Marder, S. R.; Perry, J. W. *Nature* **1999**, *398*, 51−54.

(8) Kawata, S.; Kawata, Y. *Chem. Rev.* **2000**, *100*, 1777−1788.

(9) Gu, M.; Li, X.; Cao, Y. *Light: Sci. Appl.* **2014**, *3*, e177.

(10) Denk, W.; Strickler, J.; Webb, W. *Science* **1990**, *248*, 73−76.

(11) Helmchen, F.; Denk, W. *Nat. Methods* **2005**, *2*, 932−940.

(12) Kawakami, R.; Sawada, K.; Sato, A.; Hibi, T.; Kozawa, Y.; Sato, S.; Yokoyama, H.; Nemoto, T. *Sci. Rep.* **2013**, *3*, 1014.

(13) Brown, S. B.; Brown, E. A.; Walker, I. *Lancet Oncol.* **2004**, *5*, 497−508.

(14) Goodwin, A. P.; Mynar, J. L.; Ma, Y.; Fleming, G. R.; Fréchet, J. M. J. *J. Am. Chem. Soc.* **2005**, *127*, 9952−9953.

(15) Rumi, M.; Ehrlich, J. E.; Heikal, A. A.; Perry, J. W.; Barlow, S.; Hu, Z.; McCord-Maughon, D.; Parker, T. C.; Röckel, H.; Thayumanavan, S.; Marder, S. R.; Beljonne, D.; Brédas, J.-L. *J. Am. Chem. Soc.* **2000**, *122*, 9500−9510.

(16) Brédas, J.-L.; Cornil, J.; Beljonne, D.; dos Santos, D. A.; Shuai, Z. *Acc. Chem. Res.* **1999**, *32*, 267−276.

(17) Beljonne, D.; Wenseleers, W.; Zojer, E.; Shuai, Z.; Vogel, H.; Pond, S. J. K.; Perry, J. W.; Marder, S. R.; Brédas, J. L. *Adv. Funct. Mater.* **2002**, *12*, 631−641.

(18) Masunov, A.; Tretiak, S. *J. Phys. Chem. B* **2004**, *108*, 899−907.

(19) Terenziani, F.; Katan, C.; Badaeva, E.; Tretiak, S.; Blanchard-Desce, M. *Adv. Mater.* **2008**, *20*, 4641−4678.

(20) Chung, S.-J.; Kim, K.-S.; Lin, T.-C.; He, G. S.; Swiatkiewicz, J.; Prasad, P. N. *J. Phys. Chem. B* **1999**, *103*, 10741−10745.

(21) Strehmel, B.; Sarker, A. M.; Detert, H. *ChemPhysChem* **2003**, *4*, 249−259.

(22) Woo, H. Y.; Liu, B.; Kohler, B.; Korystov, D.; Mikhailovsky, A.; Bazan, G. C. *J. Am. Chem. Soc.* **2005**, *127*, 14721−14729.

(23) Katan, C.; Terenziani, F.; Mongin, O.; Werts, M. H. V.; Porrès, L.; Pons, T.; Mertz, J.; Tretiak, S.; Blanchard-Desce, M. *J. Phys. Chem. A* **2005**, *109*, 3024−3037.

(24) Chung, S.-J.; Zheng, S.; Odani, T.; Beverina, L.; Fu, J.; Padilha, L. A.; Biesso, A.; Hales, J. M.; Zhan, X.; Schmidt, K.; Ye, A.; Zojer, E.; Barlow, S.; Hagan, D. J.; Van Stryland, E. W.; Yi, Y.; Shuai, Z.; Pagani, G. A.; Brédas, J.-L.; Perry, J. W.; Marder, S. R. *J. Am. Chem. Soc.* **2006**, *128*, 14444−14445.

(25) Pawlicki, M.; Collins, H. A.; Denning, R. G.; Anderson, H. L. *Angew. Chem., Int. Ed.* **2009**, *48*, 3244−3266.

(26) Rebane, A.; Drobizhev, M.; Makarov, N. S.; Beuerman, E.; Haley, J. E.; Krein, D. M.; Burke, A. R.; Flikkema, J. L.; Cooper, T. M. *J. Phys. Chem. A* **2011**, *115*, 4255−4262.

(27) Verbouwe, W.; Van der Auweraer, M.; De Schryver, F. C.; Piet, J. J.; Warman, J. M. *J. Am. Chem. Soc.* **1998**, *120*, 1319−1324.

(28) Amthor, S.; Lambert, C.; Dümmler, S.; Fischer, I.; Schelter, J. *J. Phys. Chem. A* **2006**, *110*, 5204−5214.

(29) Megerle, U.; Selmaier, F.; Lambert, C.; Riedle, E.; Lochbrunner, S. *Phys. Chem. Chem. Phys.* **2008**, *10*, 6245−6251.

(30) Terenziani, F.; Painelli, A.; Katan, C.; Charlot, M.; Blanchard-Desce, M. *J. Am. Chem. Soc.* **2006**, *128*, 15742−15755.

(31) Terenziani, F.; Sissa, C.; Painelli, A. *J. Phys. Chem. B* **2008**, *112*, 5079−5087.

(32) Sissa, C.; Parthasarathy, V.; Drouin-Kucma, D.; Werts, M. H. V.; Blanchard-Desce, M.; Terenziani, F. *Phys. Chem. Chem. Phys.* **2010**, *12*, 11715−11727.

(33) Terenziani, F.; Przhonska, O. V.; Webster, S.; Padilha, L. A.; Slominsky, Y. L.; Davydenko, I. G.; Gerasov, A. O.; Kovtun, Y. P.; Shandura, M. P.; Kachkovski, A. D.; Hagan, D. J.; Van Stryland, E. W.; Painelli, A. *J. Phys. Chem. Lett.* **2010**, *1*, 1800−1804.

(34) Vauthey, E. *ChemPhysChem* **2012**, *13*, 2001−2011.

(35) Carlotti, B.; Benassi, E.; Spalletti, A.; Fortuna, C. G.; Elisei, F.; Barone, V. *Phys. Chem. Chem. Phys.* **2014**, *16*, 13984−13994.

(36) Carlotti, B.; Benassi, E.; Fortuna, C. G.; Barone, V.; Spalletti, A.; Elisei, F. *ChemPhysChem* **2016**, *17*, 136−146.

(37) Li, Z.; Siklos, M.; Pucher, N.; Cicha, K.; Ajami, A.; Husinsky, W.; Rosspeintner, A.; Vauthey, E.; Gescheidt, G.; Stampfl, J.; Liska, R. *J. Polym. Sci., Part A: Polym. Chem.* **2011**, *49*, 3688−3699.

(38) Korzycka, K. A.; Bennett, P. M.; Cueto-Diaz, E. J.; Wicks, G.; Drobizhev, M.; Blanchard-Desce, M.; Rebane, A.; Anderson, H. L. *Chem. Sci.* **2015**, *6*, 2419−2426.

(39) Siebrand, W.; Williams, D. F. *J. Chem. Phys.* **1968**, *49*, 1860−1871.

(40) Englman, R.; Jortner, J. *Mol. Phys.* **1970**, *18*, 145−164.

(41) Marcus, R. A.; Sutin, N. *Biochim. Biophys. Acta, Rev. Bioenerg.* **1985**, *811*, 265−322.

(42) Nafie, L. A. *J. Phys. Chem. A* **2004**, *108*, 7222−7231.

(43) Terenziani, F.; Painelli, A. *Phys. Chem. Chem. Phys.* **2015**, *17*, 13074−13081.

(44) Hamm, P.; Ohline, S. M.; Zinth, W. *J. Chem. Phys.* **1997**, *106*, 519−529.

(45) Keane, P. M.; Wojdyla, M.; Doorley, G. W.; Watson, G. W.; Clark, I. P.; Greetham, G. M.; Parker, A. W.; Towrie, M.; Kelly, J. M.; Quinn, S. J. *J. Am. Chem. Soc.* **2011**, *133*, 4212−4215.

(46) Koch, M.; Rosspeintner, A.; Adamczyk, K.; Lang, B.; Dreyer, J.; Nibbering, E. T. J.; Vauthey, E. *J. Am. Chem. Soc.* **2013**, *135*, 9843−9848.

(47) van Stokkum, I. H. M.; Larsen, D. S.; van Grondelle, R. *Biochim. Biophys. Acta, Bioenerg.* **2004**, *1657*, 82−104.

(48) Delor, M.; Keane, T.; Scattergood, P. A.; Sazanovich, I. V.; Greetham, G. M.; Towrie, M.; Meijer, A. J. H. M.; Weinstein, J. A. *Nat. Chem.* **2015**, *7*, 689−695.

(49) Horng, M. L.; Gardecki, J. A.; Papazyan, A.; Maroncelli, M. *J. Phys. Chem.* **1995**, *99*, 17311−17337.

(50) Delor, M.; Scattergood, P. A.; Sazanovich, I. V.; Parker, A. W.; Greetham, G. M.; Meijer, A. J. H. M.; Towrie, M.; Weinstein, J. A. *Science* **2014**, *346*, 1492−1495.

DOI: 10.1021/jacs.6b01362
J. Am. Chem. Soc. 2016, 138, 4643−4649